ATMOSPHERIC SCIENCE

Global inland-water oxygen cycle has changed in the Anthropocene

Junjie Wang[1]*, Xiaochen Liu[1,2]*, Alexander F. Bouwman[1], Lauriane Vilmin[1,2], Arthur H.W. Beusen[1,3], José M. Mogollón[4], Wim J. van Hoek[1], Jack J. Middelburg[1]

Inland waters are an important resource, a highly diverse habitat, and a key component of global biogeochemical cycles. Oxygen plays a major role in inland-water ecosystem functioning, but long-term changes in its cycling remain unknown. Here, we quantify global inland-water oxygen production, consumption, and exchange with the atmosphere during 1900–2010 using a spatially explicit, mass-balanced, mechanistic model that takes into account changes in climate, hydrology, human activities, and the coupled biogeochemical (oxygen-nutrient-organic matter) dynamics. The model results show that global inland-water oxygen turnover increased during 1900–2010: production from 0.16 to 0.94 Pg year^{-1} and consumption from 0.44 to 1.47 Pg year^{-1}. Inland waters overall remained heterotrophic and a sink of atmospheric oxygen. Direct human perturbations (changes in hydrology and nutrient supply) were more important in increasing oxygen turnover than indirect effects via warming.

INTRODUCTION

Oxygen is crucial to sustaining the life of organisms in aquatic environments (*1*). Oxygen in aquatic environments influences redox processes (*2*), nutrient biogeochemistry (*3–5*), production and consumption of greenhouse gases (*6*, *7*), water quality (*8*, *9*), biological activities (*10*, *11*), and ecosystem health (*12*, *13*). Oxygen can be produced by primary producers via photosynthesis and consumed by a series of processes including respiration of organisms, decomposition of organic matter, and nitrification (*14*). As a dissolved gas, oxygen in waters readily exchanges with the atmosphere according to its saturation state (*14*). Oxygen cycling is linked to that of other biogenic elements such as carbon, nitrogen, phosphorus, silicon, and sulfur (*15–21*). However, global inland-water oxygen cycling is less studied and understood compared with that of carbon, nitrogen, phosphorus, and silicon.

Over the past decades, nutrient mobilization from various terrestrial sources to inland waters has rapidly increased due to the ever-increasing population, food production, fertilizer use, intensification and expansion of agricultural land, and wastewater discharge (*22–24*). The nutrient enrichment in inland waterbodies across the globe has caused eutrophication and algal blooms (*25*, *26*). The subsequent decay of algal detritus often depletes oxygen in the water (*27–29*). This can cause secondary problems such as fish kills, biodiversity loss, shift in community structure (to more hypoxia-tolerant species), and habitat degradation (*10*, *12*, *13*), and can trigger internal sedimentary nutrient release, which exacerbates eutrophication and related environmental problems (*30–32*).

Meanwhile, terrestrial soil loss and organic matter loading to global inland waters have increased due to changes in climate and land use (*33*, *34*). The decomposition of allochthonous organic matter in inland waters further consumes oxygen during lateral transport. Moreover, human perturbations of inland-water networks (*35*), such as damming rivers and water withdrawal for irrigation, have prolonged water travel time (*36*) and increased organic matter trapping (*37*), causing a shift in inland-water biogeochemical conditions prone to oxygen-consuming processes.

Inland-water oxygen cycling is also impacted by global warming at an unprecedented rate (*38*). Dissolved oxygen concentrations in inland waterbodies tend to be lower with rising temperature (*39*, *40*) because higher temperature reduces oxygen solubility, enhances algal production of organic matter, stimulates biogeochemical activities that decompose organic matter and consume oxygen, and limits vertical transport of water and substances (*41–44*). Increased nutrients and temperature can induce increases in both inland-water oxygen production (by enhancing primary production) and inland-water oxygen consumption (by stimulating aerobic respiration, organic matter remineralization, and nitrification). However, it remains unclear whether and how the oxygen cycling in global inland waters has changed due to these compounded global changes.

Recent studies report declining oxygen concentrations in inland-water systems such as lakes and streams (*40*, *45–47*), and machine learning has been used to identify the environmental factors governing oxygen concentrations at different temporal and spatial scales (*39*, *48*). These observation-based analyses advance our predictive capabilities of oxygen conditions in many inland-water systems, the hotspot locations and extent of short-term hypoxia events and their spatial correlation with specific environmental factors. However, these studies with the focus on oxygen concentrations have limited capabilities in advancing our understanding of global oxygen cycling mechanisms in inland waters, particularly their long-term changing dynamics and the coupling with nutrient loading, organic matter accumulation, temperature, and flow regimes in a world under unprecedented human impacts.

Process-based models are instrumental in improving our understanding of inland-water interactive transformation flows of bioactive elements and their interconnections with the land, atmosphere, and ocean. They have been developed and used for resolving the spatiotemporal changes in carbon, nitrogen, phosphorus, and silicon cycling as a result of compounded changes in climate, watershed hydrology, and human activities (*34*, *49–52*). A mechanistic perspective from process-based approaches is lacking but imperative to quantitatively understand the role of inland waters in the global

[1]Department of Earth Sciences, Utrecht University, Utrecht 3584CB, Netherlands. [2]Department of Data Science and Water Quality, Deltares, Delft 2600MH, Netherlands. [3]PBL Netherlands Environmental Assessment Agency, The Hague 2500GH, Netherlands. [4]Department of Industrial Ecology, Leiden University, Leiden 2300RA, Netherlands.
*Corresponding author. Email: j.wang3@uu.nl (J.W.); xiaochen.liu@deltares.nl (X.L.)

oxygen cycle and to answer the questions of whether, when, where, how, and why global inland-water oxygen cycling has changed.

A better understanding of inland-water oxygen cycling is essential to fill the knowledge gap and reveal the inland-water ecosystem metabolism changes due to multiple anthropogenic stressors (*53*). It also helps to better constrain the interconnected inland-water biogeochemical cycles of carbon, nitrogen, phosphorus, silicon, and other elements (*3*, *18*) and to close their global budgets across the reservoirs of the land, atmosphere, inland waters, and ocean. So far inland-water oxygen cycling and its indicated ecosystem metabolic states are not included in the assessment reports of Intergovernmental Panel on Climate Change or in Earth System Models to predict historical and future carbon cycle and associated climate feedbacks, which limits the development of more efficient and robust climate change mitigation strategies.

Here, we aim to answer the crucial questions by quantifying the dynamic global inland-water oxygen cycling (production, consumption, exchange with the atmosphere, and transport to the ocean) from the "nearly natural" 1900s (before substantial anthropogenic perturbations) to the present (2010) using the global spatially explicit, fully mass-balanced, integrated, mechanistic inland-water biogeochemistry model—Integrated Model to Assess the Global Environment–Dynamic Global Nutrient Model (IMAGE-DGNM) (Fig. 1 and fig. S1) (*49*). This process-based model explicitly resolves the feedback of inland-water oxygen cycling to changes in the supply of oxygen and nutrients from atmospheric deposition and various terrestrial sources; transport of water and its carried oxygen, nutrients, organic matter, and sediments along the aquatic continuum; and coupled biogeochemical transformation processes of oxygen with nutrients and organic matter within inland waters (see Materials and Methods for more details).

Extensive validation for the model's coupled nutrient dynamics (including that of oxygen) and hydrology have been reported in previous publications (see summary in table S1). Our site-to-site, year-by-year comparisons for a range of major river basins worldwide (covering different continents, climate zones, hydrology, and human activities) since the 1920s showcase the agreement of the simulated oxygen concentrations, chlorophyll-*a* concentrations, and

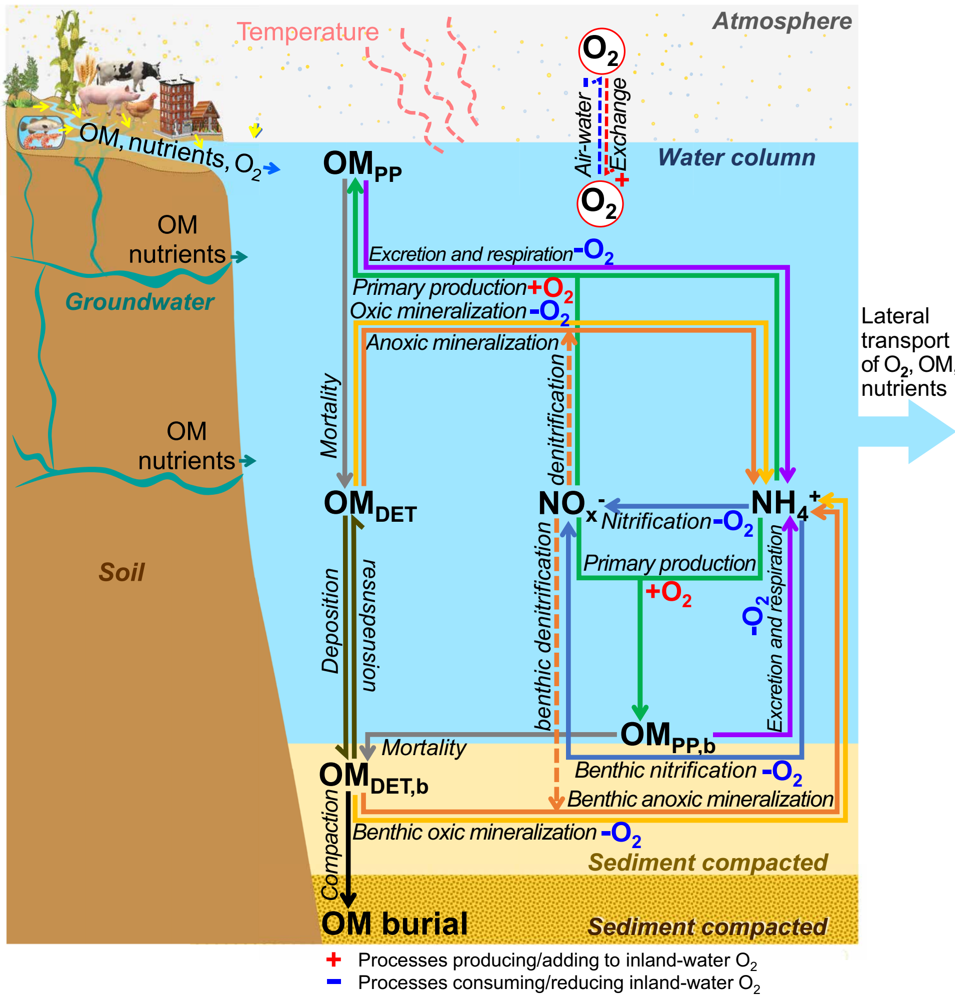

Fig. 1. Model scheme of the dynamic inland-water coupled biogeochemical flows and processes in the IMAGE-DGNM. The benthic elemental forms are not transported downstream. In the figure, "O_2" represents oxygen, processes marked with $+O_2$ and $-O_2$ represent the processes producing and consuming oxygen, respectively, "NH_4^+" represents ammonium, "NO_x^-" represents the sum of nitrate and nitrite, "OM" represents organic matter, OM_{PP} and $OM_{PP,b}$ represent organic matter generated by pelagic and benthic primary producers, respectively, and OM_{DET} and $OM_{DET,b}$ represent detrital organic matter in the water column and sediments, respectively.

hydrological flows with observations (figs. S2 and S3, and table S2). Further validation is provided by comparing oxygen metabolism estimates with observations at the system scale (fig. S4) and by consistency with global estimates on inland-water carbon cycling and nitrification (table S3). A detailed model uncertainty analysis is also presented (table S4). Then, we assess the simulated long-term evolution of global inland-water oxygen cycling from 1900 to 2010, examine its drivers using hypothetical factor-controlled scenarios, present the historical trajectory of inland-water ecosystem metabolism, and discuss the role of inland waters in the global oxygen cycle.

RESULTS AND DISCUSSION

Oxygen production in global inland waters

During 1900–2010, the simulated global inland-water oxygen production increased nearly sixfold from 0.16 to 0.94 Pg O_2 year^{-1} (Fig. 2A). Before the 1950s, this increase was slow, and was followed by a rapid increase during the 1950s–1990s and a more tempered increase in recent times. Furthermore, oxygen production shifted from predominantly benthic production (77%) in the 1900s toward mainly pelagic production (63%) in 2010 (fig. S5, A and B) despite high spatial heterogeneity (fig. S5C). The shift from a benthic toward a pelagic dominance in oxygen production occurred in the late 1970s during the fastest increase in oxygen production rates (Fig. 2A and fig. S6A).

Nutrients have strongly influenced inland-water primary production. The increasing pattern of simulated inland-water oxygen production is similar to the increase in nutrient loading to inland waters from 27 to 68 Tg nitrogen year^{-1} during 1900–2010 (Fig. 2 and fig. S8A). Simulation of inland-water oxygen cycling under a scenario with unchanged nutrient loading to inland waters after the 1900s shows that oxygen production would increase threefold over the 110-year period (to 0.50 Pg year^{-1} in 2010; Table 1). This indicates that without the 1900–2010 increase in nutrient loading, the increase rate of oxygen production would be 56% less (than the base scenario with the historical nutrient loading increase).

The Anthropocene has also seen alterations to the water cycle. With the growing number of constructed reservoirs since 1900 (fig. S8D), our model shows that the contributions of lentic waters to global inland-water oxygen production increased from 53% in the 1900s to 85% in 2010 (fig. S7A). Under the base scenario with impacts of increased water residence time during 1900–2010, nutrient regeneration from organic matter mineralization within inland waters increased by more than threefold (*50*), serving as an internal nutrient supply that fueled increased oxygen production. Under the scenario of oxygen cycling with unchanged hydrology (i.e., inland-water volume, area, and discharge) after the 1900s, the present-day oxygen production would be 0.29 Pg year^{-1}, which indicates that the oxygen production increase without the historical increase in water residence time would be more than 80% (0.66 Pg year^{-1}) less (Table 1).

Warmer temperature can increase aquatic primary production (*54*, *55*). Under another scenario of oxygen cycling with unchanged temperature after the 1900s, the simulated present-day oxygen production would be 0.85 Pg year^{-1}, i.e., 11% (0.09 Pg year^{-1}) lower than the base scenario under which the global annual average temperature increased by 1.4°C during 1900–2010 (fig. S8E). This warming-enhanced oxygen production increase has been observed in warming temperate lakes (*45*).

The 1900–2010 historical changes in external nutrient loading, warming, and water residence time synergistically account for 97% of the simulated oxygen production increase compared to the 1900s (Table 1). However, as these anthropogenic pressures have different focal points on the global scale, there are some important spatial patterns in oxygen production changes that have emerged. In 1900, before intensifying human impacts, the largest inland-water oxygen production was in humid warm areas such as Amazon, Orinoco, Parana, Congo, and island basins in Asia and Oceania (Fig. 2B), where vigorous natural vegetations delivered substantial nutrients to surface waters (*22*). In 2010, the highest inland-water oxygen production extended beyond these natural hotspots to regions receiving

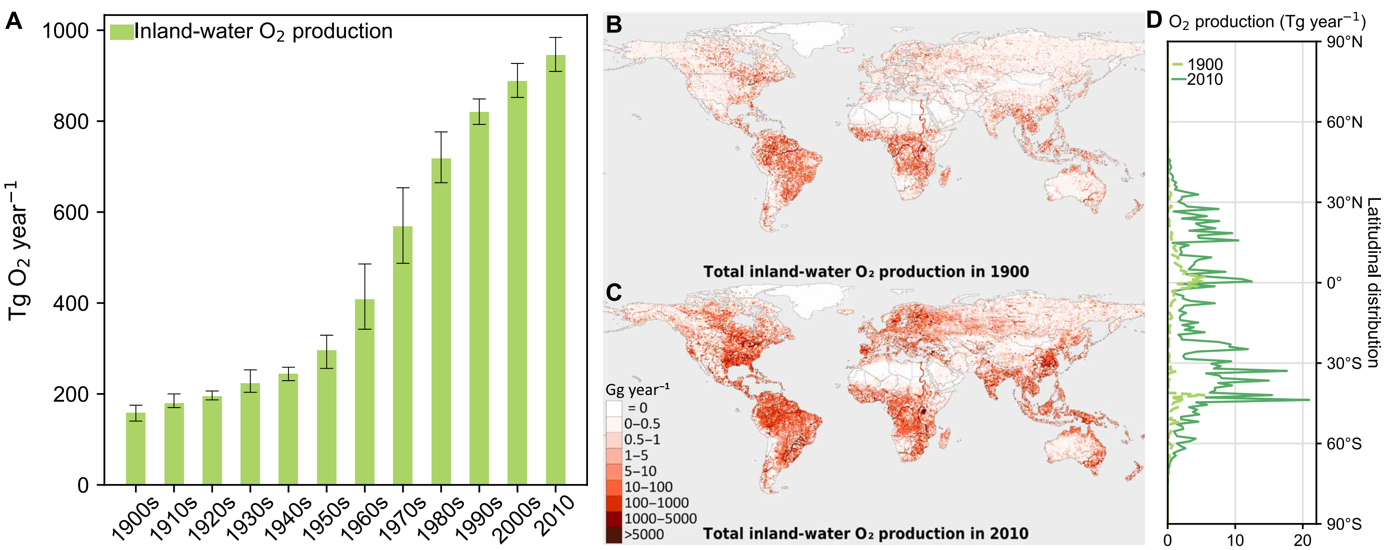

Fig. 2. Spatiotemporal changes in the simulated global oxygen production in inland waters during 1900–2010. Temporal changes during 1900–2010 (**A**), spatial distributions at a resolution of 0.5° × 0.5° in 1900 (**B**) and 2010 (**C**), and latitudinal distributions in both years (**D**). The ranges in (A) indicate intradecadal variations. In the figures, "Tg year^{-1}" represents teragrams per year, and "Gg year^{-1}" represents gigagrams per year.

Table 1. Comparison of the simulated present-day inland-water oxygen cycling under the base scenario and under scenarios with a single driver (among temperature, external nutrient loading, and hydrology, respectively) unchanged and with the three major drivers unchanged after the 1900s. Note that all oxygen flows are rounded to 0.01 Pg year^{-1}. Δ and its following numbers in parentheses represent the temporal changes in the present-day oxygen flows compared with those in the 1900s before intensifying human perturbations. δ and its following numbers in parentheses represent the differences in the present-day oxygen flows between the base scenario (with compounded historical changes during 1900–2010) and those simulated under the scenarios controlled with a single driver unchanged or three drivers unchanged since the 1900s. The controlled drivers are temperature, external nutrient loading, and water residence time. See Materials and Methods for more details.

Period	Scenarios	Inland-water oxygen cycling (Pg year^{-1})				
		External oxygen input	Oxygen production	Oxygen consumption	Oxygen exchange with the atmosphere	River oxygen export to the ocean
1900s	Before intensifying human perturbations	0.01	0.16	0.44	0.66	0.37
Present-day period (represented by the year 2010)	Base scenario (with compounded historical changes during 1900–2010)	0.02 (Δ = +0.01)	0.94 (Δ = +0.79)	1.47 (Δ = +1.03)	0.95 (Δ = +0.29)	0.42 (Δ = +0.05)
	Scenario with unchanged temperature after the 1900s	0.02 (Δ = +0.01) **(δ = −0.00)**	0.85 (Δ = +0.69) **(δ = −0.09)**	1.30 (Δ = +0.96) **(δ = −0.17)**	0.82 (Δ = +0.16) **(δ = −0.12)**	0.38 (Δ = +0.01) **(δ = −0.04)**
	Scenario with unchanged external nutrient loading after the 1900s	0.02 (Δ = +0.01) **(δ = −0.00)**	0.50 (Δ = +0.34) **(δ = −0.44)**	0.78 (Δ = +0.34) **(δ = −0.69)**	0.71 (Δ = +0.04) **(δ = −0.25)**	0.42 (Δ = +0.05) **(δ = +0.00)**
	Scenario with unchanged water volume, area, and discharge after the 1900s	0.02 (Δ = +0.01) **(δ = −0.00)**	0.29 (Δ = +0.13) **(δ = −0.66)**	0.85 (Δ = +0.41) **(δ = −0.63)**	0.93 (Δ = +0.27) **(δ = −0.02)**	0.36 (Δ = −0.01) **(δ = −0.06)**
	Scenario with unchanged external nutrient loading, temperature, and hydrology (water volume, area and discharge) after the 1900s	0.02 (Δ = +0.01) **(δ = −0.00)**	0.18 (Δ = +0.02) **(δ = −0.77)**	0.46 (Δ = +0.02) **(δ = -1.02)**	0.66 (Δ = +0.01) **(δ = −0.28)**	0.37 (Δ = −0.00) **(δ = −0.04)**

large anthropogenic nutrient loading from agriculture and wastewater discharge (fig. S8), such as southeastern North America, western and central Europe, southern and eastern Asia, coastal Oceania, central and southern Africa, and eastern South America, but more concentrated in mainstream channels and downstream reaches (Fig. 2C and fig. S9A). This spatial concentration of oxygen production may be related to the availability of inorganic nutrient forms in watersheds, which supports photosynthesis. While organic forms dominate nutrient loading to watersheds (*56*), recent studies show that due to inland-water transformations, the inorganic proportion downstream increases during the nutrient transport along the aquatic continuum (*49*–*52*), and these inland-water transformations are enhanced by the prolonged residence time due to damming rivers (*50*, *57*). The increased availability of inorganic nutrients downstream thus enhances local oxygen production.

Throughout the period 1900–2010, the lowest inland-water oxygen production mainly occurred in low-temperature (e.g., Greenland, northern Asia, and northwestern North America) and dry regions (e.g., northern and southwestern Africa, central Oceania, and western Asia) (Fig. 2, B and C). However, with warming, increased nutrient loading, and damming rivers worldwide, inland-water oxygen production has become prevalent, extending toward higher latitudes (Fig. 2D). In 1900, tropical zones contributed the most to global inland-water oxygen production, while in 2010, the largest contributing regions shifted to subtropical and temperate zones in the southern Hemisphere.

Oxygen consumption in global inland waters

During 1900–2010, the simulated global inland-water oxygen consumption increased from 0.44 to 1.47 Pg year^{-1} (Fig. 3A). Oxygen consumption in both the water column and sediments increased (fig. S5). Benthic processes dominated total oxygen consumption in the entire 110-year period, although its proportion overall decreased from 82 to 60% (fig. S5, A and B) and showed high spatial variability (fig. S5F).

Our model results show that the inland-water oxygen consumption was mainly caused by aerobic mineralization of (allochthonous and autochthonous) organic matter, followed by nitrification and respiration of algae (fig. S6). During 1900–2010, aerobic mineralization of organic matter, nitrification, and algal respiration increased by a factor of 3, 4, and 9 during 1900–2010, respectively (fig. S6). The shares of nitrification (from 14% to 17%) and algal respiration (from 6% to 16%) in total oxygen consumption increased at the expense of aerobic mineralization of organic matter, which declined from 80 to 67%.

Since the 1900s, the delivery of allochthonous organic matter from terrestrial to inland-water systems nearly doubled (fig. S8B), which is less rapid than the sixfold increase in autochthonous inland-water organic production (as is also indicated by inland-water oxygen production discussed above; Fig. 2). Under the scenario with unchanged nutrient loading to inland waters after the 1900s, the simulated oxygen consumption would increase less than twofold over the 110-year period (Table 1). This indicates that the increase rate of total oxygen consumption would be 67% less than the base scenario with the historical increase in nutrient loading. This is because with the increased availability of allochthonous and autochthonous organic matter in inland waters during 1900–2010 (fig. S8B), inland waters function as an active reactor transforming organic to inorganic carbon via mineralization of organic matter and

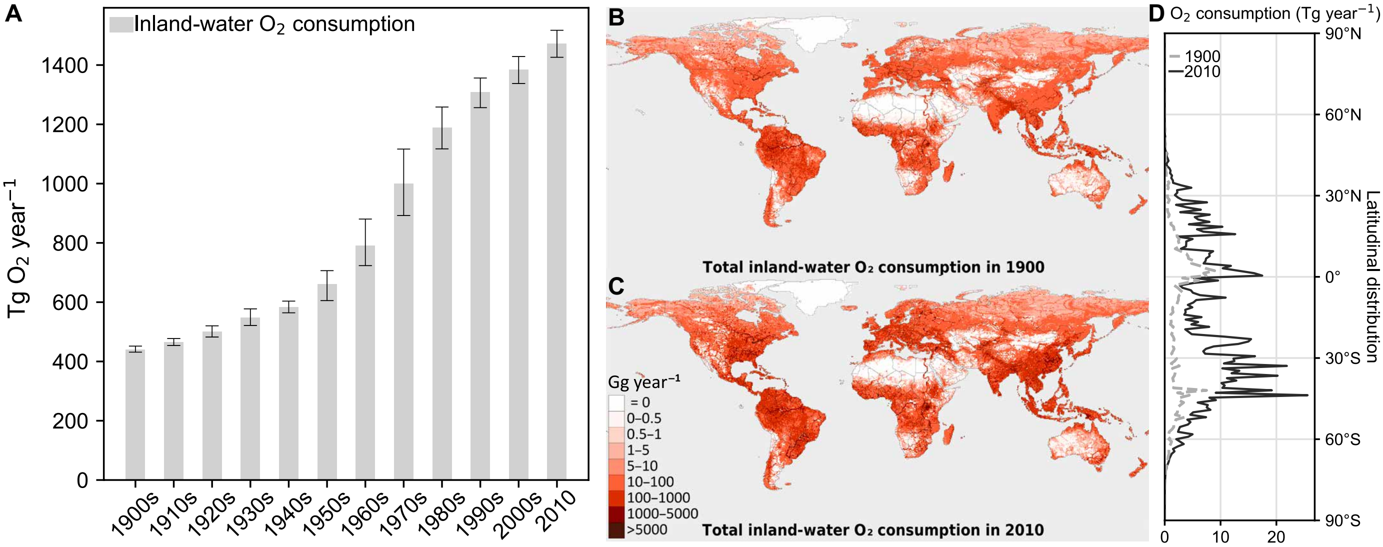

Fig. 3. Spatiotemporal changes in the simulated global oxygen consumption in inland waters during 1900–2010. Temporal changes during 1900–2010 (**A**), spatial distributions at a resolution of 0.5° × 0.5° in 1900 (**B**) and 2010 (**C**), and latitudinal distributions in both years (**D**). The ranges in (A) indicate intradecadal variations.

respiration (*49*–*52*), during which oxygen consumption was largely enhanced.

The prolonged water residence time due to damming has not only enhanced increases in simulated oxygen and internal organic production (Fig. 2 and fig. S8B) but has also increased oxygen consumption (Table 1). This is because damming increases organic matter trapping and prolongs the time for biogeochemical processes within inland-water systems, which largely enhances oxygen consumption by mineralization. Consequently, the contributions of lentic waters to global inland-water oxygen consumption increased nearly threefold, from 22% in the 1900s to 60% in 2010 (fig. S7B). The present-day oxygen consumption under the scenario with unchanged hydrology (i.e., inland-water volume, area, and discharge) after the 1900s would be 0.85 Pg year^{-1}, i.e., 0.6 Pg year^{-1} (~60%) lower than that under the base scenario with historical changes in hydrology (Table 1).

Global warming can also increase mineralization of organic matter (*58*, *59*). The simulated present-day total oxygen consumption would be 1.30 Pg year^{-1} under the scenario with unchanged temperature after the 1900s, i.e., 0.17 Pg year^{-1} lower than that under the base scenario with historical warming (Table 1). This 16% decline in oxygen consumption due to absence of historical warming is consistent with observed higher oxygen consumption in warming environments (*44*, *45*, *60*).

The historical changes in external organic matter and nutrient loading, warming, and water residence time during 1900–2010 synergistically account for 98% of the simulated oxygen consumption increase compared to the 1900s (Table 1). As with oxygen production, the spatial patterns of inland-water oxygen consumption also reflect anthropogenic activities. Oxygen consumption tends to follow the patterns of nutrient loading (Fig. 3, B and C, and fig. S8), which is high in large agricultural areas and population centers across watersheds. The external nutrient loading is mainly organic (*56*) and can directly fuel in situ oxygen consumption, so that oxygen consumption is more extensively distributed within watersheds compared with the scattered pattern of oxygen production. Nevertheless, our results show that hotspots of high oxygen production in mainstream channels and downstream reaches (Fig. 2, B and C) are also hotspots of high oxygen consumption fueled by locally produced organic matter. As a result of the increased external organic matter delivery, global warming, and enhanced organic production due to anthropogenic nutrient loading and prolonged water residence time, the simulated oxygen consumption increased in most of the global inland waters during 1900–2010 (Fig. 3, B to D, and fig. S9B). The increase in temperate and subtropical zones tends to be larger than that in tropical and frigid zones, and the highest oxygen consumption moved from tropical zones to subtropical and temperate zones in the Southern Hemisphere, where the large surface water areas with long residence time received increased external inputs of nutrients and organic matter.

Inland-water oxygen cycling

Global inland waters are a sink for atmospheric oxygen in the Anthropocene. The simulated influx from the atmosphere increased from 0.66 Pg year^{-1} in the 1900s to 0.95 Pg year^{-1} in 2010 (Fig. 4 and fig. S6). The present-day oxygen uptake from the atmosphere is similar to oxygen production in inland waters (Fig. 4D). However, this was not always the case during the evaluated 110-year span, especially in the period before intensified and expanded human impacts. In the 1900s, oxygen uptake from the atmosphere was four times as much as inland-water oxygen production because oxygen production was largely limited by nutrient availability (Fig. 4A).

Because of increased external nutrient and organic matter supply from terrestrial systems, warming, and hydrology changes, both oxygen production and consumption rates have increased but at different rates. The ratio of simulated inland-water oxygen production to consumption was lower than 1 during the entire period of 1900–2010 (Fig. 4C). At the start of the 20th century, oxygen production was only one-third of oxygen consumption. In contrast, the present-day oxygen production balances two-thirds of the oxygen consumption. Although the ratio of simulated oxygen production to consumption has been increasing due to a faster increase in nutrient than organic matter supply from land, the net oxygen production in inland waters, i.e., the difference between oxygen production and consumption (also referred to as net ecosystem production), has become increasingly negative from −0.3 Pg year^{-1} in the 1900s to −0.5 Pg year^{-1} in 2010 (Fig. 4B). This estimate of overall negative net oxygen production is consistent with the Odum's metabolic framework (*61*, *62*) and the extensively documented ecosystem-scale heterotrophic state of global inland waters (*63*–*65*) and many individual systems (*53*, *54*, *60*–*62*, *66*, *67*), despite varying extents across regions (*54*, *60*, *66*, *67*). The pronounced net heterotrophy of inland waters is also reflected by their carbon dioxide effluxes (*34*, *54*, *63*–*65*, *68*). Our estimated present-day net ecosystem production (−0.5 Pg O_2 year^{-1}) in global inland waters falls within the range of previous estimates using carbon fluxes (−0.2 to −0.3 Pg carbon year^{-1} or −0.4 to −0.7 Pg O_2 year^{-1}; table S3) (*34*, *63*–*65*). Moreover, our revealed increasingly negative net oxygen production in global inland waters aligns with the warming-induced decrease in net ecosystem production in continental-scale streams (table S3) (*60*). While the simulated global oxygen production and consumption are close to balance in the water column, oxygen is invading inland waters to compensate for the net sedimentary oxygen consumption (fig. S5). Although lentic waters have become increasingly active in both oxygen production and consumption processes, our model shows that most of the global inland-water oxygen exchange with the atmosphere has occurred in lotic waters during the evaluated 110-year period (fig. S7). This indicates the importance of inland waters in the global oxygen cycle as both reactors and transporters.

Without the synergistic impacts of historical changes in external organic matter and nutrient loading, warming, and hydrology, the simulated inland-water oxygen cycling in the present day and the 1900s would be very similar (Table 1). The present-day inland-water oxygen uptake from the atmosphere would be 0.1 Pg year^{-1} higher under the base scenario with historical warming (fig. S8E) than under the scenario with unchanged temperature after the 1900s (Table 1). This is mainly because historical warming has stimulated a larger increase in the present-day inland-water oxygen consumption (+0.2 Pg year^{-1}) than in oxygen production (+0.1 Pg year^{-1}), which is similar to the previously predicted decrease of 0.06 Pg year^{-1} in net oxygen production in streams under 1°C warming (table S3) (*60*).

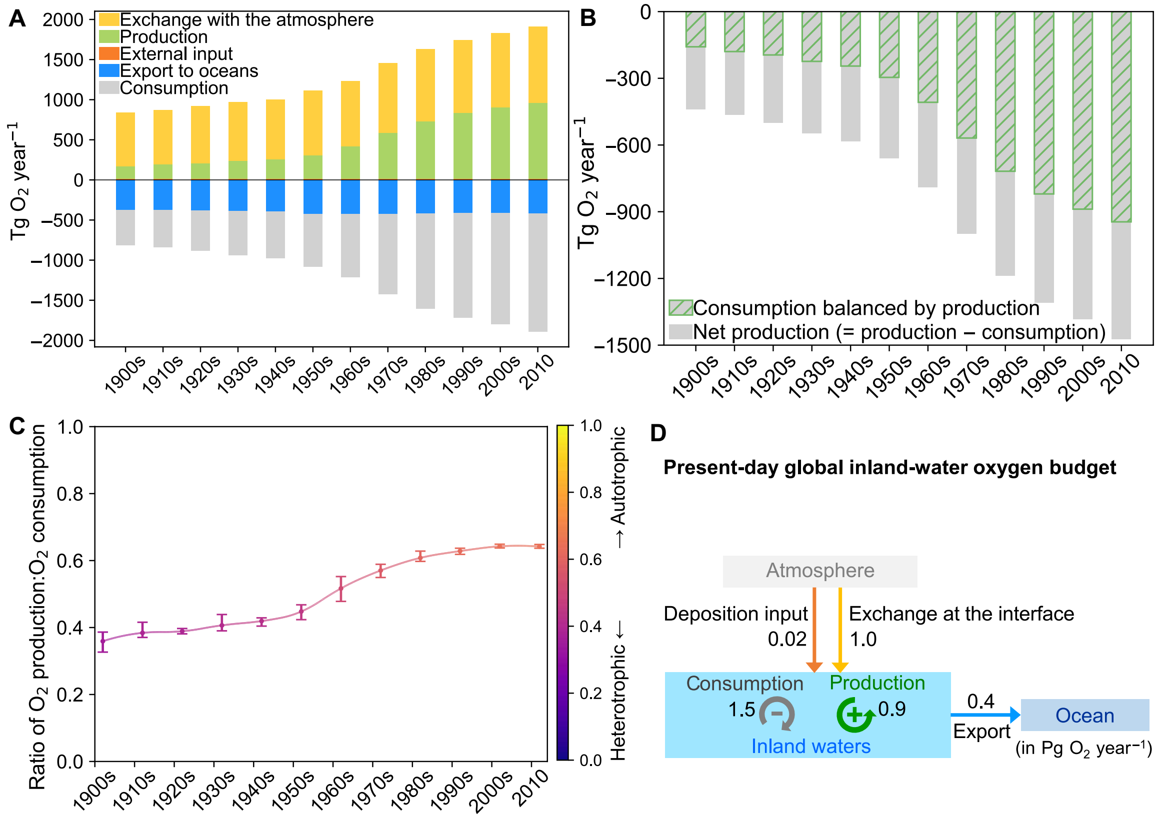

Fig. 4. Changes in the simulated global inland-water oxygen cycling and implications for inland-water ecosystem metabolisms and the global oxygen budget. Temporal changes in the simulated global inland-water oxygen cycling budget (**A**), net oxygen production (i.e., the difference between oxygen production and consumption) in inland waters (**B**), the ratio of inland-water oxygen production to consumption during 1900–2010 (**C**), and the role of inland waters in the present-day (represented by the year 2010) global oxygen budget in terms of interactions with the atmosphere and the ocean (**D**). In (A), external oxygen input (in orange) is almost invisible because this external input has been negligible (less than 5%) compared with oxygen production, consumption, atmospheric exchange, and export to oceans (see details in fig. S6). In (B), the full gray column indicates the total inland-water oxygen consumption, the green-hatched part indicates the part of oxygen consumption balanced by total oxygen production, and the lowermost gray part indicates the (negative) net oxygen production resulting from their difference. The ranges in (C) indicate intradecadal variations.

Likewise, the simulated present-day inland-water oxygen uptake from the atmosphere would be 0.2 Pg year^{-1} higher under the base scenario (with the historical growth in nutrient loading) (fig. S8) than under the scenario with unchanged nutrient loading after the 1900s (Table 1). This is balanced by the difference in the present-day net oxygen production between the base scenario (more negative −0.5 Pg year^{-1}) and the scenario with unchanged nutrient loading after the 1900s (−0.3 Pg year^{-1}).

In contrast, the simulated present-day inland-water oxygen uptake from the atmosphere would be rather similar with or without the historical changes in hydrology (i.e., inland-water volume, area, and discharge) after the 1900s (Table 1). This change in oxygen uptake from the atmosphere related to historical hydrology changes is very small (0.02 Pg year^{-1}) because the increases in the present-day oxygen production (+0.66 Pg year^{-1}) and consumption (+0.63 Pg year^{-1}) due to historical hydrology changes nearly balance each other.

The simulated transport of oxygen dissolved in river water to global oceans has been rather constant (0.4 Pg year^{-1}) during 1900–2010 (Fig. 4A). Existing estimates of river oxygen export are rare but consistent with ours. The global biogeochemical mass-balanced budget model TOTEM estimated river oxygen export of 0.4 Pg year^{-1} for the year 2000 based on riverine carbon and nitrogen fluxes and their fixed ratios to oxygen (*69*). Duursma and Boisson (*70*) estimated 0.3 Pg year^{-1} of river oxygen export in the 1980s based on the assumption that world rivers had an average oxygen concentration of 8 mg/liter and total water discharge to oceans of 3.7×10^4 km^3 year^{-1} (*71*).

Implications for global oxygen budget

Although the inland-water surface area is only 0.2% of the ocean area (*72*, *73*), the present-day inland-water oxygen uptake of 0.95 Pg year^{-1} is estimated to be about half the quantity of net oxygen degassing from the ocean to the atmosphere [1.74 Pg year^{-1} in Huang *et al.* (*74*); 1.6 Pg year^{-1} in Li *et al.* (*75*)] and 1.7-fold the 0.56 Pg year^{-1} of oxygen uptake in the global coast zone (*69*), and could lower the unaccounted global oxygen sink from 2.69 (*74*) to 1.74 Pg year^{-1}. It is important to highlight that this inland-water oxygen uptake from the atmosphere is not included in existing global oxygen budgets (*69*, *74*) and that river oxygen export to oceans is often excluded (*74*, *75*).

While inland waters play an important role in the present-day global oxygen budget, our model shows that inland-water oxygen cycling has markedly changed during 1900–2010 under increasing anthropogenic impacts. Compared with the "nearly natural" inland-water oxygen cycling in the 1900s, inland-water oxygen production, consumption, and uptake from the atmosphere have largely increased but at different rates (Fig. 4). The 110-year increases in inland-water oxygen flows are of the same or larger magnitudes of the "nearly natural" inland-water oxygen flows in the 1900s. The changed inland-water oxygen cycle—which closely interacts with the atmosphere, land, and ocean—is an indication of the alteration of the entire global oxygen cycle in the Anthropocene. For example, the increasing inland-water oxygen uptake from the atmosphere under anthropogenic stresses is consistent with the increasing terrestrial oxygen uptake from the atmosphere, which is also human driven (*74*). These increasing oxygen sinks in terrestrial and inland-water systems, in turn, correspond to the oxygen declines in the atmosphere (*76*) and the ocean (*77*) since the 20th century. Including the temporal changes driven by anthropogenic perturbations and distinguishing between "nearly natural" and "present-day" global oxygen budget are therefore critical because the oxygen cycle is interconnected with ecosystem metabolism and the evolution of the Earth system (*1*, *78*), and a robust assessment of its temporal trajectory profoundly influences the understanding of the Earth's habitability in the past and the projected future.

Using simulations of the process-based IMAGE-DGNM model, this study shows that inland waters are a large, growing, and spatially concentrated sink for atmospheric oxygen. Global inland-water oxygen consumption may continue to increase in the coming future, considering the projected warming (*38*), perturbations to hydrology (*79*), and nutrient loading from present-day and historical practices (*80*). Not only oxygen budget and inventory estimates, but also policies aiming at addressing the long-term aggravation of inland-water ecosystem health, need to take into account inland-water oxygen cycling flows, their spatial and temporal variabilities, and underlying drivers. These inland-water oxygen cycling changes would cause cascading impacts on the interconnected cycling of carbon and nutrients (*3*–*6*, *81*), expansion and intensification of inland-water hypoxia (*82*, *83*), and increases in greenhouse-gas emissions (*44*, *84*, *85*) that contribute to climate change. To halt or reverse this trend, policy implementation to mitigate warming as well as environmental and agricultural management to reduce nutrient loading are urgent, particularly in the hotspots of inland-water oxygen sink with much higher oxygen consumption than production.

Notably, this study only focuses on the long-term changes over the l10-year period, while the short-term (seasonal, monthly, or daily) dynamics may also contribute to the variability of oxygen cycling. It is possible that temperature or other factors are predominant drivers of seasonal and daily oxygen cycle changes, such as vertical stratification (*44*, *86*). These subannual changes, however, are beyond the focus of this study. Including short-timescale inland-water oxygen dynamics in future modeling efforts will further enhance our understanding of global oxygen cycling under extreme events (e.g., floods, droughts, and heatwaves) (*87*–*89*) and better predict seasonal ecosystem impacts of deep-water hypoxia (*40*, *44*, *90*).

MATERIALS AND METHODS

The model used: IMAGE-DGNM

We used the IMAGE-DGNM model to quantify the evolving inland-water oxygen biogeochemical cycling on the global scale. The IMAGE-DGNM is a spatially explicit, process-based, mass-balanced model that couples various natural and anthropogenic sources and processes on land and soils [IMAGE (*91*)], hydrological balance and processes across river network [PCRaster Global Water Balance (PCR-GLOBWB); (*92*, *93*)], and dynamic biogeochemical processes in inland waters [Dynamic In-Stream Chemistry module (DISC); (*49*)]. IMAGE-DGNM (*34*, *49*–*52*, *94*) explicitly simulates the dynamic inland-water biogeochemical cycling of nitrogen, phosphorus, silicon, carbon, and oxygen in inland-water systems driven by changes in land cover, climate, population, agriculture, aquaculture, wastewater discharge, atmospheric deposition, water use, and perturbance of hydrology such as damming rivers and construction of reservoirs.

In IMAGE-DGNM, the IMAGE model (*91*) simulates long-term grid-based land cover, climate, population, water use, and human activities, and the hydrology model PCR-GLOBWB simulates the long-term grid-based runoff, discharge, water area, and volume in different waterbodies (including streams, lakes, and reservoirs) for each year (*92*, *93*), with the calculation of stream orders in each grid for each year based on the method of Wollheim *et al.* (*95*). Data of lake characteristics are from the Global Lakes and Wetlands Database (*96*), and data of reservoir characteristics are from the Global Reservoir and Dam database (*35*) and dynamically introduced based on their reported construction year. IMAGE-DGNM uses the coupling of IMAGE and PCR-GLOBWB to calculate the long-term, grid-based nutrient, oxygen, carbon, and sediment delivery fluxes per year and to couple the process-based DISC module for simulating the long-term, grid-based, mass-balanced dynamic biogeochemistry of nitrogen, phosphorus, silicon, carbon, and oxygen in inland waters for each year (*34*, *49*–*52*, *94*) (Fig. 1 and fig. S1). All data used and model components have a consistent 0.5 × 0.5° spatial resolution.

The inland-water dynamics of oxygen, organic matter, different nutrient forms, and sediments is depicted in a coupled, mass-balanced, and internally consistent manner in the mechanistic DISC module of IMAGE-DGNM (*49*, *50*, *94*). In this study, organic matter is expressed in organic nitrogen (ON), nutrients forms include ammonium (NH_4^+), nitrate + nitrite ($NO_x^- = NO_2^- + NO_3^-$), and ON, and sediments include those suspended in the water column (total suspended solids in the water column, TSS) and those settled in the benthic layer (total benthic sediments in the uncompacted layer, TBS).

For each waterbody type (stream, river, lake, or reservoir) within a 0.5° × 0.5° grid cell, changes in the amount of inland-water oxygen per 1-year time step depend on oxygen input to the waterbody (from headwaters within the grid, upstream grids, and atmospheric deposition input from rainfall; text S1), hydrological oxygen transport flux from the waterbody to the downstream, inland-water oxygen production and consumption, and oxygen exchange at the water-atmosphere interface. Inland-water oxygen production is from photosynthesis of pelagic and benthic primary producers. Inland-water oxygen consumption includes respiration of pelagic and benthic primary producers, aerobic mineralization in the water column and sediments, and nitrification in the water column and sediments. Detailed methodology and equations can be found in text S1.

The dynamic reaction rates of each inland-water process are subject to change depending on the contemporaneous environmental conditions (such as temperature, hydrology, loading, and concentrations of different nutrient forms and oxygen, organic matter accumulation, sediment dynamics, and coupled interactions; see text S1) specific to that time, location, and waterbody. In this study, the model output time step is 1 year, while biogeochemical processes are solved implicitly using an adaptive time step (≤0.5 year). The full IMAGE-DGNM model description including the solving methodology and equations for inland-water oxygen biogeochemical processes can be found in (*49*, *50*, *94*).

All model parameters and model inputs are from previous studies (*49*, *50*, *56*, *80*, *94*, *97*). Note that IMAGE-DGNM analysis of performance, including exhaustive validation analyses against global measurements (of hydrology, nutrients, carbon, dissolved oxygen, sediment, and trace gas) at different spatial and temporal scales and model sensitivity analyses, was previously performed (*22*, *34*, *49*–*52*, *80*, *94*, *97*–*102*).

Oxygen cycling in factor-controlled scenarios

In this study, we assessed the relative importance of warming, growth in external nutrient loading, and prolonged water residence time (due to changes in inland-water volume, area and discharge) since the 1900s individually and synergistically, and their consequences for the simulated present-day inland-water oxygen cycling. In contrast to the base scenario (which incorporates the compounded historical changes in climate, hydrology and anthropogenic nutrient loading during 1900–2010), under each of the controlled scenarios, one driver among temperature, external nutrient loading, and hydrology was assumed to be unchanged since the 1900s to simulate the changes in inland-water oxygen cycling during 1900–2010. Therefore, with the same initial state before intensifying human perturbations in the 1900s, the inland-water oxygen cycling would evolve differently because of the absence of the change in the single driver. The differences between the simulated present-day inland-water oxygen cycling flows under the base scenario and under the scenario controlled with unchanged temperature/external nutrient loading/hydrology (water volume, area, discharge, and resulting residence time) since the 1900s were used to explore the influences of historical warming, growth in external nutrient loading, and prolonged water residence time related to hydrology changes individually. In addition, to evaluate the compounding effect, the three drivers (temperature, external nutrient loading, and hydrology) were kept unchanged since the 1900s as a fourth scenario to simulate the changes in inland-water oxygen cycling during 1900–2010 and to examine the synergistic effect of the historical changes in these three drivers.

It is important to recognize that the conclusion about the relative importance of different drivers may be specific to the annual and longer timescales. It is possible that temperature or other factors are predominant drivers of seasonal and daily oxygen cycle changes, such as stratification (*44*, *86*). This subannual change is beyond the focus of this study on the drivers of the 110-year long-term oxygen cycling change in the Anthropocene.

Data for validation: Site-to-site, year-by-year, major river basins, and long-term trends

We collected long-term site-level observational data of dissolved oxygen concentration, chlorophyll-*a* concentration, and water discharge for a range of major river basins worldwide since the 1920s from literature and databases (table S2) including United States Geological Survey (*103*), Water Quality Portal (*104*), Department of Water and Sanitation, South Africa (*105*), Global River Chemistry Database (*106*), and Global Freshwater Quality Database (*107*) to validate our coupled oxygen biogeochemistry model. These sites and river basins cover different continents and different climate zones and represent a range in hydrology and human activity (e.g., economic development levels, population, land use, and dam construction). For dissolved oxygen concentration, chlorophyll-*a* concentration, and water discharge, we performed comparisons of simulations and observations site-to-site year-by-year, examined their long-term trends, and calculated multiple statistical metrics—including mean-normalized root mean squared error (NRMSE), percent bias (Pbias in %), and coefficient of determination (R^2)—to further evaluate the model performance (text S2 and figs. S2 and S3).

The validation results showcase the agreement of the simulated oxygen concentrations, chlorophyll-*a* concentrations, and hydrological flows with observations site-to-site, year-by-year for a range of major river basins worldwide since the 1920s (figs. S2 and S3, and table S2). Their long-term trends are well represented, generally with NRMSE below 1, Pbias below 100 (%), and R^2 exceeding 0.5 (figs. S2 and S3). The discrepancy between simulations and observations may be partly due to differences in their temporal and spatial representativity. While simulations on the annual basis may miss the short-term variations within the year, the annual means of observational data may be limited in representing the annual average due to potentially incomplete temporal coverage and/or uneven distribution of observations within each compared year, although we used observational data for years with at least 4 months of observations to reduce related influences. The coarse resolution (0.5° × 0.5°) of the model simulations may not fully capture the internal spatial heterogeneity within the grid cell, while the available site-level observations may not accurately reflect the average condition of the entire grid cell.

We further validated the model by comparing our simulated and the observation-based estimates of inland-water net oxygen production (i.e., net ecosystem production represented in oxygen, which is the difference between inland-water oxygen production and consumption) for the present-day period at both the site level (fig. S4) and on the global scale (table S3). Validations for the model's coupled nutrient dynamics (including that of oxygen) and hydrology were extensively performed in previous publications, with a summary in table S1.

Sensitivity and uncertainty analyses

To enhance understanding of the uncertainties in our modeling of global inland-water oxygen cycling, we evaluated the sensitivity of the simulated fluxes of oxygen production, consumption, net production, exchange with the atmosphere, and export to the ocean to the variations in 9 environmental forcings, 7 terrestrial inputs (of oxygen, various nutrient forms, and TSS), and 64 model parameters. This analysis examines how the variations in these 80 model inputs, constraints, and parameters collectively drive changes in inland-water oxygen cycling. The Latin hypercube sampling approach was used to generate 800 random sets of parameters within the high-dimensional parameter space (via USATOOL) (*108*). Accordingly, we conducted 800 model simulations using these generated sets of inputs and parameters. We then quantified the sensitivity of simulated oxygen process fluxes to the variations in parameters using the standardized regression coefficient [SRC; see the detailed SRC methodology description in our publications (*49*, *52*, *97*)]. Ultimately, eight inputs and parameters were identified as having a significant and important influence (SRC > 0.2 or SRC < -0.2, corresponding to an influence exceeding 4%) on at least one of the simulated oxygen process fluxes in global inland waters (table S4A and details in text S3).

The SD in percentage was used to quantify the relative uncertainty ranges of the simulated oxygen process fluxes induced by the assumed variation ranges of all model inputs, constraints, and parameters (table S4B and details in text S3). Results show that the calculated relative uncertainty ranges vary among the fluxes of different oxygen processes (table S4B). The relative uncertainty ranges of inland-water oxygen exchange with the atmosphere, consumption, net oxygen production, and export to the ocean are smaller than that of inland-water oxygen production. Inland-water oxygen cycling processes tend to vary similarly or less than the imposed variations in inputs and model parameters.

Supplementary Materials

This PDF file includes:
Supplementary Texts S1 to S3
Tables S1 to S4
Figs. S1 to S9
References

REFERENCES AND NOTES

1. H. Decker, K. E. Holde, *Oxygen and the Evolution of Life*. (Springer, 2011).
2. B. Sundby, L. G. Anderson, P. O. J. Hall, Å. Iverfeldt, M. M. R. van der Loeff, S. F. G. Westerlund, The effect of oxygen on release and uptake of cobalt, manganese, iron and phosphate at the sediment-water interface. *Geochim. Cosmochim. Acta* **50**, 1281–1288 (1986).
3. C. C. Carey, P. C. Hanson, R. Q. Thomas, A. B. Gerling, A. G. Hounshell, A. S. L. Lewis, M. E. Lofton, R. P. McClure, H. L. Wander, W. M. Woelmer, B. R. Niederlehner, M. E. Schreiber, Anoxia decreases the magnitude of the carbon, nitrogen, and phosphorus sink in freshwaters. *Glob. Chang. Biol.* **28**, 4861–4881 (2022).
4. S. Müller, S. M. Mitrovic, D. S. Baldwin, Oxygen and dissolved organic carbon control release of N, P and Fe from the sediments of a shallow, polymictic lake. *J. Soils Sediments* **16**, 1109–1120 (2016).
5. L.-R. Nteziryayo, Å. Danielsson, Sediment DSi and DIP fluxes under changing oxygen availability in bottom waters. *Boreal Environ. Res.* **23**, 159–174 (2018).
6. A. Liikanen, T. Murtoniemi, H. Tanskanen, T. Väisänen, P. J. Martikainen, Effects of temperature and oxygen availability on greenhouse gas and nutrient dynamics in sediment of a eutrophic mid-boreal lake. *Biogeochemistry* **59**, 269–286 (2002).
7. M. S. Rosamond, S. J. Thuss, S. L. Schiff, Dependence of riverine nitrous oxide emissions on dissolved oxygen levels. *Nat. Geosci.* **5**, 715–718 (2012).
8. E. Sánchez, M. F. Colmenarejo, J. Vicente, A. Rubio, M. G. García, L. Travieso, R. Borja, Use of the water quality index and dissolved oxygen deficit as simple indicators of watersheds pollution. *Ecol. Indic.* **7**, 315–328 (2007).
9. P. R. Kannel, S. Lee, Y.-S. Lee, S. R. Kanel, S. P. Khan, Application of water quality indices and dissolved oxygen as indicators for river water classification and urban impact assessment. *Environ. Monit. Assess.* **132**, 93–110 (2007).
10. P. B. Moyle, J. J. Cech Jr, *Fishes: An introduction to ichthyology*. P. B. Moyle, J. J. Cech Jr, Eds. (Pearson Prentice Hall, 2004).
11. R. G. Wetzel, *Limnology. Lake and river ecosystems* (Academic Press, ed. 3, 2001), pp. 1006.
12. M. M. Dorgham, in *Eutrophication: Causes, Consequences and Control.* A. A. Ansari, S. S. Gill, Eds. (Springer, 2014), pp. 29–44. vol. 2.
13. G. N. Saari, Z. Wang, B. W. Brooks, Revisiting inland hypoxia: diverse exceedances of dissolved oxygen thresholds for freshwater aquatic life. *Environ. Sci. Pollut. Res.* **25**, 3139–3150 (2018).
14. B. Cox, A review of dissolved oxygen modelling techniques for lowland rivers. *Sci. Total Environ.* **314-316**, 303–334 (2003).
15. J. Emsley, in *The Natural Environment and the Biogeochemical Cycles,* O. Hutzinger, Ed. (Springer, 1980), pp. 147–167.
16. K. Wallmann, G. Aloisi, "The global carbon cycle: Geological processes," in *Fundamentals of Geobiology*, A. H. Knoll, D. E. Canfield, K. O. Konhauser Eds. (Wiley, 2012), pp. 20–35.
17. A. J. B. Zehnder, S. H. Zinder, in *The Natural Environment and the Biogeochemical Cycles,* O. Hutzinger, Ed. (Springer, 1980), pp. 105–145.
18. B. Shao, R. Zhang, X. Xu, L. Niu, K. Fan, Z. Lin, L. Zhao, X. Zhou, N. Ren, D.-J. Lee, C. Chen, Cryptic sulfur and oxygen cycling potentially reduces N_2O-driven greenhouse warming: underlying revision need of the nitrogen cycle. *Environ. Sci. Technol.* **56**, 5960–5972 (2022).
19. I. Berman-Frank, Y.-B. Chen, Y. Gao, K. Fennel, M. Follows, A. Milligan, P. Falkowski, "Feedbacks between the nitrogen, carbon and oxygen cycles," in *Nitrogen in the Marine Environment*, D. G. Capone, D. A. Bronk, M. R. Mulholland, E. J. Carpenter, Eds., (Academic Press, 2008), vol. 35, pp. 1537–1563.
20. P. G. Falkowski, *Life's Engines: How Microbes Made Earth Habitable*. P. G. Falkowski, Ed., (Princeton Uni. Press, 2023).
21. D. E. Canfield, "*Oxygen: A Four Billion Year History*," (Princeton Univ. Press, 2014), vol. 20.
22. A. H. W. Beusen, A. F. Bouwman, L. P. H. Van Beek, J. M. Mogollón, J. J. Middelburg, Global riverine N and P transport to ocean increased during the 20th century despite increased retention along the aquatic continuum. *Biogeosciences* **13**, 2441–2451 (2016).
23. J. N. Galloway, F. J. Dentener, D. G. Capone, E. W. Boyer, R. W. Howarth, S. P. Seitzinger, G. P. Asner, C. C. Cleveland, P. A. Green, E. A. Holland, D. M. Karl, A. F. Michaels, J. H. Porter, A. R. Townsend, C. J. Vörösmarty, Nitrogen cycles: Past, present, and future. *Biogeochemistry* **70**, 153–226 (2004).
24. S. P. Seitzinger, E. Mayorga, A. F. Bouwman, C. Kroeze, A. H. W. Beusen, G. Billen, G. Van Drecht, E. Dumont, B. M. Fekete, J. Garnier, J. A. Harrison, Global river nutrient export: A scenario analysis of past and future trends. *Global Biogeochem. Cycles* **24**, 01–14 (2010).
25. V. H. Smith, G. D. Tilman, J. C. Nekola, Eutrophication: Impacts of excess nutrient inputs on freshwater, marine, and terrestrial ecosystems. *Environ. Pollut.* **100**, 179–196 (1999).
26. N. N. Rabalais, Nitrogen in aquatic ecosystems. *Ambio* **31**, 102–112 (2002).
27. J.-P. Jenny, A. Normandeau, P. Francus, Z. E. Taranu, I. Gregory-Eaves, F. Lapointe, J. Jautzy, A. E. K. Ojala, J.-M. Dorioz, A. Schimmelmann, B. Zolitschka, Urban point sources of nutrients were the leading cause for the historical spread of hypoxia across European lakes. *Proc. Natl. Acad. Sci. U.S.A.* **113**, 12655–12660 (2016).

28. L. L. Yuan, J. R. Jones, Modeling hypolimnetic dissolved oxygen depletion using monitoring data. *Can. J. Fish. Aquat. Sci.* **77**, 814–823 (2020).
29. D. M. Anderson, P. M. Glibert, J. M. Burkholder, Harmful algal blooms and eutrophication: Nutrient sources, composition, and consequences. *Estuaries* **25**, 704–726 (2002).
30. R. P. North, R. L. North, D. M. Livingstone, O. Köster, R. Kipfer, Long-term changes in hypoxia and soluble reactive phosphorus in the hypolimnion of a large temperate lake: consequences of a climate regime shift. *Glob. Chang. Biol.* **20**, 811–823 (2014).
31. L. Zhang, S. Wang, Z. Wu, Coupling effect of pH and dissolved oxygen in water column on nitrogen release at water–sediment interface of Erhai Lake, China. *Estuar. Coast. Shelf Sci.* **149**, 178–186 (2014).
32. J. J. Middelburg, L. A. Levin, Coastal hypoxia and sediment biogeochemistry. *Biogeosciences* **6**, 1273–1293 (2009).
33. P. Regnier, L. Resplandy, R. G. Najjar, P. Ciais, The land-to-ocean loops of the global carbon cycle. *Nature* **603**, 401–410 (2022).
34. W. J. van Hoek, J. Wang, L. Vilmin, A. H. W. Beusen, J. M. Mogollón, G. Müller, P. A. Pika, X. Liu, J. J. Langeveld, A. F. Bouwman, J. J. Middelburg, Exploring spatially explicit changes in carbon budgets of global river basins during the 20th century. *Environ. Sci. Technol.* **55**, 16757–16769 (2021).
35. B. Lehner, C. Reidy Liermann, C. Revenga, C. Vörösmarty, B. Fekete, P. Crouzet, P. Döll, M. Endejan, K. Frenken, J. Magome, C. Nilsson, J. C. Robertson, R. Rödel, N. Sindorf, D. Wisser, High-resolution mapping of the world's reservoirs and dams for sustainable river-flow management. *Front. Ecol. Environ.* **9**, 494–502 (2011).
36. C. J. Vörösmarty, K. P. Sharma, B. M. Fekete, A. H. Copeland, J. Holden, J. Marble, J. A. Lough, The storage and aging of continental runoff in large reservoir systems of the world. *Ambio* **26**, 210–219 (1997).
37. P. J. Mulholland, J. W. Elwood, The role of lake and reservoir sediments as sinks in the perturbed global carbon cycle. *Tellus* **34**, 490–499 (1982).
38. IPCC, "Climate Change 2021: The Physical Science Basis. Contribution of Working Group I to the Sixth Assessment Report of the Intergovernmental Panel on Climate Change," (2021).
39. W. Zhi, W. Ouyang, C. Shen, L. Li, Temperature outweighs light and flow as the predominant driver of dissolved oxygen in US rivers. *Nat. Water* **1**, 249–260 (2023).
40. J. R. Blaszczak, L. E. Koenig, F. H. Mejia, L. Gómez-Gener, C. L. Dutton, A. M. Carter, N. B. Grimm, J. W. Harvey, A. M. Helton, M. J. Cohen, Extent, patterns, and drivers of hypoxia in the world's streams and rivers. *Limnol. Oceanogr. Lett.* **8**, 453–463 (2023).
41. D. Tromans, Temperature and pressure dependent solubility of oxygen in water: a thermodynamic analysis. *Hydrometallurgy* **48**, 327–342 (1998).
42. H. Seki, M. Takahashi, Y. Hara, S. Ichimura, Dynamics of dissolved oxygen during algal bloom in Lake Kasumigaura, Japan. *Water Res.* **14**, 179–183 (1980).
43. G. Yvon-Durocher, J. I. Jones, M. Trimmer, G. Woodward, J. M. Montoya, Warming alters the metabolic balance of ecosystems. *Philos. Trans. R. Soc. Lond. B Biol. Sci.* **365**, 2117–2126 (2010).
44. S. F. Jane, J. L. Mincer, M. P. Lau, A. S. L. Lewis, J. T. Stetler, K. C. Rose, Longer duration of seasonal stratification contributes to widespread increases in lake hypoxia and anoxia. *Glob. Chang. Biol.* **29**, 1009–1023 (2023).
45. S. F. Jane, G. J. A. Hansen, B. M. Kraemer, P. R. Leavitt, J. L. Mincer, R. L. North, R. M. Pilla, J. T. Stetler, C. E. Williamson, R. I. Woolway, L. Arvola, S. Chandra, C. L. DeGasperi, L. Diemer, J. Dunalska, O. Erina, G. Flaim, H.-P. Grossart, K. D. Hambright, C. Hein, J. Hejzlar, L. L. Janus, J.-P. Jenny, J. R. Jones, L. B. Knoll, B. Leoni, E. Mackay, S.-I. S. Matsuzaki, C. McBride, D. C. Müller-Navarra, A. M. Paterson, D. Pierson, M. Rogora, J. A. Rusak, S. Sadro, E. Saulnier-Talbot, M. Schmid, R. Sommaruga, W. Thiery, P. Verburg, K. C. Weathers, G. A. Weyhenmeyer, K. Yokota, K. C. Rose, Widespread deoxygenation of temperate lakes. *Nature* **594**, 66–70 (2021).
46. J.-P. Jenny, P. Francus, A. Normandeau, F. Lapointe, M.-E. Perga, A. Ojala, A. Schimmelmann, B. Zolitschka, Global spread of hypoxia in freshwater ecosystems during the last three centuries is caused by rising local human pressure. *Glob. Chang. Biol.* **22**, 1481–1489 (2016).
47. W. Zhi, C. Klingler, J. Liu, L. Li, Widespread deoxygenation in warming rivers. *Nat. Clim. Chang.* **13**, 1105–1113 (2023).
48. R. Barzegar, M. T. Aalami, J. Adamowski, Short-term water quality variable prediction using a hybrid CNN–LSTM deep learning model. *Stoch. Env. Res. Risk A.* **34**, 415–433 (2020).
49. L. Vilmin, J. M. Mogollón, A. H. W. Beusen, W. J. van Hoek, X. Liu, J. J. Middelburg, A. F. Bouwman, Modeling process-based biogeochemical dynamics in surface fresh waters of large watersheds with the IMAGE-DGNM framework. *J. Adv. Model. Earth Syst.* **12**, e2019MS001796 (2020).
50. J. Wang, A. F. Bouwman, L. Vilmin, A. H. W. Beusen, W. J. van Hoek, X. Liu, J. J. Middelburg, Global inland-water nitrogen cycling has accelerated in the Anthropocene. *Nat. Water* **2**, 729–740 (2024).
51. L. Vilmin, A. F. Bouwman, A. H. W. Beusen, W. J. van Hoek, J. M. Mogollón, Past anthropogenic activities offset dissolved inorganic phosphorus retention in the Mississippi River basin. *Biogeochemistry* **161**, 157–169 (2022).
52. X. Liu, W. J. van Hoek, L. Vilmin, A. H. W. Beusen, J. M. Mogollon, J. J. Middelburg, A. F. Bouwman, Exploring long-term changes in silicon *Biogeochemistry* along the river continuum of the Rhine and Yangtze (Changjiang). *Environ. Sci. Technol.* **54**, 11940–11950 (2020).
53. E. R. Hotchkiss, T. DelSontro, in *Wetzel's Limnology* I. D. Jones, J. P. Smol, Eds. (Academic Press, San Diego, 4th ed., 2024), pp. 939–997.
54. B. O. L. Demars, G. M. Gíslason, J. S. Ólafsson, J. R. Manson, N. Friberg, J. M. Hood, J. J. D. Thompson, T. E. Freitag, Impact of warming on CO_2 emissions from streams countered by aquatic photosynthesis. *Nat. Geosci.* **9**, 758–761 (2016).
55. G. Yvon-Durocher, A. P. Allen, J. M. Montoya, M. Trimmer, G. Woodward, "The temperature dependence of the carbon cycle in aquatic ecosystems," in *Advances in Ecological Research* (Academic Press, 2010), vol. 43, pp. 267–313.
56. L. Vilmin, J. M. Mogollón, A. H. W. Beusen, A. F. Bouwman, Forms and subannual variability of nitrogen and phosphorus loading to global river networks over the 20th century. *Glob. Planet. Chang.* **163**, 67–85 (2018).
57. A. F. Bouwman, M. F. P. Bierkens, J. Griffioen, M. M. Hefting, J. J. Middelburg, H. Middelkoop, C. P. Slomp, Nutrient dynamics, transfer and retention along the aquatic continuum from land to ocean: towards integration of ecological and biogeochemical models. *Biogeosciences* **10**, 1–22 (2013).
58. S. W. Duan, S. S. Kaushal, Warming increases carbon and nutrient fluxes from sediments in streams across land use. *Biogeosciences* **10**, 1193–1207 (2013).
59. C. Gudasz, D. Bastviken, K. Steger, K. Premke, S. Sobek, L. J. Tranvik, Temperature-controlled organic carbon mineralization in lake sediments. *Nature* **466**, 478–481 (2010).
60. C. Song, W. K. Dodds, J. Rüegg, A. Argerich, C. L. Baker, W. B. Bowden, M. M. Douglas, K. J. Farrell, M. B. Flinn, E. A. Garcia, A. M. Helton, T. K. Harms, S. Jia, J. B. Jones, L. E. Koenig, J. S. Kominoski, W. H. McDowell, D. McMaster, S. P. Parker, A. D. Rosemond, C. M. Ruffing, K. R. Sheehan, M. T. Trentman, M. R. Whiles, W. M. Wollheim, F. Ballantyne, Continental-scale decrease in net primary productivity in streams due to climate warming. *Nat. Geosci.* **11**, 415–420 (2018).
61. T. J. Hoellein, D. A. Bruesewitz, D. C. Richardson, Revisiting Odum (1956): A synthesis of aquatic ecosystem metabolism. *Limnol. Oceanogr.* **58**, 2089–2100 (2013).
62. H. T. Odum, Primary production in flowing waters. *Limnol. Oceanogr.* **1**, 102–117 (1956).
63. T. J. Battin, L. A. Kaplan, S. Findlay, C. S. Hopkinson, E. Marti, A. I. Packman, J. D. Newbold, F. Sabater, Biophysical controls on organic carbon fluxes in fluvial networks. *Nat. Geosci.* **1**, 95–100 (2008).
64. T. J. Battin, R. Lauerwald, E. S. Bernhardt, E. Bertuzzo, L. G. Gener, R. O. Hall, E. R. Hotchkiss, T. Maavara, T. M. Pavelsky, L. Ran, P. Raymond, J. A. Rosentreter, P. Regnier, River ecosystem metabolism and carbon *Biogeochemistry* in a changing world. *Nature* **613**, 449–459 (2023).
65. P. Regnier, P. Friedlingstein, P. Ciais, F. T. Mackenzie, N. Gruber, I. A. Janssens, G. G. Laruelle, R. Lauerwald, S. Luyssaert, A. J. Andersson, S. Arndt, C. Arnosti, A. V. Borges, A. W. Dale, A. Gallego-Sala, Y. Goddéris, N. Goossens, J. Hartmann, C. Heinze, T. Ilyina, F. Joos, D. E. LaRowe, J. Leifeld, F. J. R. Meysman, G. Munhoven, P. A. Raymond, R. Spahni, P. Suntharalingam, M. Thullner, Anthropogenic perturbation of the carbon fluxes from land to ocean. *Nat. Geosci.* **6**, 597–607 (2013).
66. E. S. Bernhardt, P. Savoy, M. J. Vlah, A. P. Appling, L. E. Koenig, R. O. Hall, M. Arroita, J. R. Blaszczak, A. M. Carter, M. Cohen, J. W. Harvey, J. B. Heffernan, A. M. Helton, J. D. Hosen, L. Kirk, W. H. McDowell, E. H. Stanley, C. B. Yackulic, N. B. Grimm, Light and flow regimes regulate the metabolism of rivers. *Proc. Natl. Acad. Sci. U.S.A.* **119**, e2121976119 (2022).
67. N. S. Marzolf, M. Ardón, Ecosystem metabolism in tropical streams and rivers: a review and synthesis. *Limnol. Oceanogr.* **66**, 1627–1638 (2021).
68. J. J. Cole, Y. T. Prairie, N. F. Caraco, W. H. McDowell, L. J. Tranvik, R. G. Striegl, C. M. Duarte, P. Kortelainen, J. A. Downing, J. J. Middelburg, J. Melack, Plumbing the global carbon cycle: Integrating inland waters into the terrestrial carbon budget. *Ecosystems* **10**, 172–185 (2007).
69. C. Rabouliie, F. T. MacKenzie, L. M. Ver, Influence of human perturbation on carbon, nitrogen, and oxygen biogeochemical cycles in the global coastal ocean. *Geochim. Cosmochim. Acta* **65**, 3615–3641 (2001).
70. E. K. Duursma, M. P. R. M. Boisson, Global oceanic and atmospheric oxygen stability considered in relation to the carbon-cycle and to different time scales. *Oceanol. Acta* **17**, 117–141 (1994).
71. V. Ittekkot, Global trends in the nature of organic matter in river suspensions. *Nature* **332**, 436–438 (1988).
72. G. H. Allen, T. M. Pavelsky, Global extent of rivers and streams. *Science* **361**, 585–588 (2018).
73. J. G. Cogley, Area of the Ocean. *Mar. Geod.* **35**, 379–388 (2012).
74. J. Huang, J. Huang, X. Liu, C. Li, L. Ding, H. Yu, The global oxygen budget and its future projection. *Sci. Bull.* **63**, 1180–1186 (2018).
75. C. Li, J. Huang, L. Ding, X. Liu, H. Yu, J. Huang, Increasing escape of oxygen from oceans under climate change. *Geophys. Res. Lett.* **47**, e2019GL086345 (2020).
76. R. Keeling, in *Scripps O2 Global Oxygen Measurements*. (Scripps Institution of Oceanography, 2023).

77. S. Schmidtko, L. Stramma, M. Visbeck, Decline in global oceanic oxygen content during the past five decades. *Nature* **542**, 335–339 (2017).
78. J. Huang, X. Liu, Y. He, S. Shen, Z. Hou, S. Li, C. Li, L. Yao, J. Huang, The oxygen cycle and a habitable Earth. *Sci. China Earth Sci.* **64**, 511–528 (2021).
79. C. Zarfl, A. E. Lumsdon, J. Berlekamp, L. Tydecks, K. Tockner, A global boom in hydropower dam construction. *Aquat. Sci.* **77**, 161–170 (2015).
80. A. H. W. Beusen, J. C. Doelman, L. P. H. Van Beek, P. J. T. M. Van Puijenbroek, J. M. Mogollón, H. J. M. Van Grinsven, E. Stehfest, D. P. Van Vuuren, A. F. Bouwman, Exploring river nitrogen and phosphorus loading and export to global coastal waters in the Shared Socio-economic pathways. *Glob. Environ. Chang.* **72**, 102426 (2022).
81. S. P. Seitzinger, J. A. Harrison, J. K. Böhlke, A. F. Bouwman, R. Lowrance, B. Peterson, C. Tobias, G. V. Drecht, Denitrification across landscapes and waterscapes: A synthesis. *Ecol. Appl.* **16**, 2064–2090 (2006).
82. M. Søndergaard, R. Bjerring, E. Jeppesen, Persistent internal phosphorus loading during summer in shallow eutrophic lakes. *Hydrobiologia* **710**, 95–107 (2013).
83. S. Ding, M. Chen, M. Gong, X. Fan, B. Qin, H. Xu, S. Gao, Z. Jin, D. C. W. Tsang, C. Zhang, Internal phosphorus loading from sediments causes seasonal nitrogen limitation for harmful algal blooms. *Sci. Total Environ.* **625**, 872–884 (2018).
84. J. Guilhen, A. Al Bitar, S. Sauvage, M. Parrens, J. M. Martinez, G. Abril, P. Moreira-Turcq, J. M. Sánchez-Pérez, Denitrification and associated nitrous oxide and carbon dioxide emissions from the Amazonian wetlands. *Biogeosciences* **17**, 4297–4311 (2020).
85. Y. Maruya, K. Nakayama, M. Sasaki, K. Komai, Effect of dissolved oxygen on methane production from bottom sediment in a eutrophic stratified lake. *J. Environ. Sci.* **125**, 61–72 (2023).
86. M. R. Andersen, T. Kragh, K. Sand-Jensen, Extreme diel dissolved oxygen and carbon cycles in shallow vegetated lakes. *Proc. Biol. Sci.* **284**, 20171427 (2017).
87. L. Gómez-Gener, A. Lupon, H. Laudon, R. A. Sponseller, Drought alters the biogeochemistry of boreal stream networks. *Nat. Commun.* **11**, 1795 (2020).
88. J. L. Kerr, D. S. Baldwin, K. L. Whitworth, Options for managing hypoxic blackwater events in river systems: A review. *J. Environ. Manag.* **114**, 139–147 (2013).
89. R. I. Woolway, E. Jennings, T. Shatwell, M. Golub, D. C. Pierson, S. C. Maberly, Lake heatwaves under climate change. *Nature* **589**, 402–407 (2021).
90. Z. Wu, D. Yu, Q. Yu, Q. Liu, M. Zhang, R. A. Dahlgren, J. J. Middelburg, L. Qu, Q. Li, W. Guo, N. Chen, Greenhouse gas emissions (CO_2–CH_4–N_2O) along a large reservoir-downstream river continuum: The role of seasonal hypoxia. *Limnol. Oceanogr.* **69**, 1015–1029 (2024).
91. E. Stehfest, D. P. Van Vuuren, T. Kram, A. F. Bouwman, *Integrated Assessment of Global Environmental Change with IMAGE 3.0. Model description and policy applications*. (PBL Netherlands Environmental Assessment Agency, 2014), pp. 370.
92. L. P. H. Van Beek, Y. Wada, M. F. P. Bierkens, Global monthly water stress: 1. Water balance and water availability. *Water Resour. Res.* **47**, W07517 (2011).
93. E. H. Sutanudjaja, R. Van Beek, N. Wanders, Y. Wada, J. H. C. Bosmans, N. Drost, R. J. Van Der Ent, I. E. M. De Graaf, J. M. Hoch, K. De Jong, D. Karssenberg, P. López López, S. Peßenteiner, O. Schmitz, M. W. Straatsma, E. Vannametee, D. Wisser, M. F. P. Bierkens, PCR-GLOBWB 2: A 5 arcmin global hydrological and water resources model. *Geosci. Model Dev.* **11**, 2429–2453 (2018).
94. J. Wang, L. Vilmin, J. M. Mogollón, A. H. W. Beusen, W. J. van Hoek, X. Liu, P. A. Pika, J. J. Middelburg, A. F. Bouwman, Inland waters increasingly produce and emit nitrous oxide. *Environ. Sci. Technol.* **57**, 13506–13519 (2023).
95. W. Wollheim, C. J. Vörösmarty, A. F. Bouwman, P. Green, J. Harrison, E. Linder, B. J. Peterson, S. P. Seitzinger, J. M. Syvitski, Global N removal by freshwater aquatic systems using a spatially distributed, within-basin approach. *Global Biogeochem. Cycles* **22**, GB2026 (2008).
96. B. Lehner, P. Döll, Development and validation of a global database of lakes, reservoirs and wetlands. *J. Hydrol.* **296**, 1–22 (2004).
97. A. H. W. Beusen, L. P. H. Van Beek, A. F. Bouwman, J. M. Mogollón, J. J. Middelburg, Coupling global models for hydrology and nutrient loading to simulate nitrogen and phosphorus retention in surface water. Description of IMAGE-GNM and analysis of performance. *Geosci. Model Dev.* **8**, 4045–4067 (2015).
98. X. Liu, A. H. W. Beusen, L. P. H. Van Beek, J. M. Mogollón, X. Ran, A. F. Bouwman, Exploring spatiotemporal changes of the Yangtze River (Changjiang) nitrogen and phosphorus sources, retention and export to the East China Sea and Yellow Sea. *Water Res.* **142**, 246–255 (2018).
99. X. Liu, A. H. W. Beusen, Impact of groundwater nitrogen legacy on water quality. *Nat. Sustain.* **7**, 891–900 (2024).
100. J. Wang, X. Liu, A. H. W. Beusen, J. J. Middelburg, Surface-water nitrate exposure to world populations has expanded and intensified during 1970–2010. *Environ. Sci. Technol.* **57**, 19395–19406 (2023).
101. A. F. Bouwman, X. Liu, A. H. W. Beusen, Exploring the global index of freshwater eutrophication potential for the period 1900–2015, paper presented at the AGU Fall Meeting, Chicago, IL, 12 to 16 December 2022.
102. J. Zhou, L. Scherer, P. M. van Bodegom, A. H. W. Beusen, J. M. Mogollón, A comparison between global nutrient retention models for freshwater systems. *Front. Water* **4**, 894604 (2022).
103. USGS (United States Geological Survey, 2022); http://waterdata.usgs.gov/nwis/qwdata [accessed 25 May 2023].
104. Water Quality Portal. Washington (DC): National Water Quality Monitoring Council, United States Geological Survey (USGS), Environmental Protection Agency (EPA) (2021). https://doi.org/10.5066/P9QRKUVJWQP
105. DWS, S. A. Department of Water and Sanitation, Research Quality Information Services, Ed. (DWS, 2022); www.dws.gov.za/iwqs/report.aspx.
106. J. Hartmann, R. Lauerwald, N. Moosdorf, GLORICH - Global river chemistry database [dataset] (PANGAEA, 2019); https://doi.pangaea.de/10.1594/PANGAEA.902360.
107. UNEP, *GEMStat database of the Global Environment Monitoring System for Freshwater (GEMS/Water) Programme,* U. N. E. Programme, Ed., (International Centre for Water Resources and Global Change, 2018); https://gemstat.bafg.de/.
108. A. Saltelli, S. Tarantola, F. Campolongo, M. Ratto, *Sensitivity analysis in practice. A guide to assessing scientific models*. (Wiley and Sons, 2004).
109. S. R. Alin, M. de Fátima F. L. Rasera, C. I. Salimon, J. E. Richey, G. W. Holtgrieve, A. V. Krusche, A. Snidvongs, Physical controls on carbon dioxide transfer velocity and flux in low-gradient river systems and implications for regional carbon budgets. *J. Geophys. Res.* **116**, 10.1029/2010JG001398 (2011).
110. R. Wanninkhof, Relationship between wind speed and gas exchange over the ocean. *J. Geophys. Res.* **97**, 7373–7382 (1992).
111. American Public Health Association (APHA), "Standard methods for the examination of water and wastewater. 4500-O oxygen (dissolved) in *Standard Methods For the Examination of Water and Wastewater*, W. C. Lipps, T. E. Baxter, E. Braun-Howland, Eds. (APHA Press, ed. 18, 1992), vol. 4.
112. M. Despotovic, V. Nedic, D. Despotovic, S. Cvetanovic, Evaluation of empirical models for predicting monthly mean horizontal diffuse solar radiation. *Renew. Sust. Energ. Rev.* **56**, 246–260 (2016).
113. J. Wang, A. H. W. Beusen, X. Liu, R. Van Dingenen, F. Dentener, Q. Yao, B. Xu, X. Ran, Z. Yu, A. F. Bouwman, Spatially explicit inventory of sources of nitrogen inputs to the Yellow Sea, East China Sea and South China Sea for the period 1970-2010. *Earth's Future* **8**, 001511–001514 (2020).
114. M. Liu, P. A. Raymond, R. Lauerwald, Q. Zhang, G. Trapp-Müller, K. L. Davis, N. Moosdorf, C. Xiao, J. J. Middelburg, A. F. Bouwman, A. H. W. Beusen, C. Peng, F. Lacroix, H. Tian, J. Wang, M. Li, Q. Zhu, S. Cohen, W. J. van Hoek, Y. Li, Y. Li, Y. Yao, P. Regnier, Global riverine land-to-ocean carbon export constrained by observations and multi-model assessment. *Nat. Geosci.* **17**, 896–904 (2024).
115. M. A. A. Jwaideh, E. H. Sutanudjaja, C. Dalin, Global impacts of nitrogen and phosphorus fertiliser use for major crops on aquatic biodiversity. *Int. J. Life Cycle Assess.* **27**, 1058–1080 (2022).
116. Ministry of Water Resources of the People's Republic of China, "Hydrological Yearbook, National water and rainfall information." (2015).
117. J. Lin, P. Wang, J. Wang, Y. Zhou, X. Zhou, P. Yang, H. Zhang, Y. Cai, Z. Yang, An extensive spatiotemporal water quality dataset covering four decades (1980–2022) in China. *Earth Syst. Sci. Data* **16**, 1137–1149 (2024).
118. Y. Chen, C. Fan, K. Teubner, M. Dokulil, Changes of nutrients and phytoplankton chlorophyll-*a* in a large shallow lake, Taihu, China: An 8-year investigation. *Hydrobiologia* **506-509**, 273–279 (2003).
119. Y. Zhang, Y. Su, J. Yu, Z. Liu, Y. Du, M. Jin, Anthropogenically driven differences in n-alkane distributions of surface sediments from 19 lakes along the middle Yangtze River, Eastern China. *Environ. Sci. Pollut. Res.* **26**, 22472–22484 (2019).
120. Q. Guan, L. Feng, X. Hou, G. Schurgers, Y. Zheng, J. Tang, Eutrophication changes in fifty large lakes on the Yangtze Plain of China derived from MERIS and OLCI observations. *Remote Sens. Environ.* **246**, 111890 (2020).
121. E. E. Van Nieuwenhuyse, Response of summer chlorophyll concentration to reduced total phosphorus concentration in the Rhine River (Netherlands) and the Sacramento–San Joaquin Delta (California, USA). *Can. J. Fish. Aquat. Sci.* **64**, 1529–1542 (2007).
122. S. P. Seitzinger, C. Kroeze, Global distribution of nitrous oxide production and N inputs in freshwater and coastal marine ecosystems. *Global Biogeochem. Cycles* **12**, 93–113 (1998).

Acknowledgements

Funding: This work was supported by EMBRACER (Summit grant SUMMIT.1.034) financed by the Netherlands Organization for Scientific Research (NWO) (to J.W. and J.J.M.), the Dutch Ministry of Education, Culture and Science through the Netherlands Earth System Science Center (NESSC) (to J.W. and J.J.M.), the ICEP indicator Development project nos. 4500462526 and WE.461002.1 funded by the World Resources Institute and UNESCO (to X.L., A.H.W.B., and A.F.B), and the PBL Netherlands Environmental Assessment Agency through in-kind contributions to The New Delta 2014 ALW projects no. 869.15.015 and 869.15.014 (to A.F.B. and A.H.W.B.). **Author contributions:** J.W. and J.J.M. conceptualized the study. J.W .and L.V. developed oxygen dynamics in DISC module. A.H.W.B., A.F.B., and J.M.M. developed the IMAGE-DGNM framework. W.J.v.H. and X.L. contributed to model components. J.W. ran the model simulations and conducted data analysis. J.W., X.L., and J.J.M. prepared the manuscript. All co-authors reviewed the manuscript. **Competing interests:** The authors declare that they

have no competing interests. **Data and materials availability:** All data needed to evaluate the conclusions in this paper are present in the paper and/or the Supplementary Materials. The data of simulated oxygen cycling fluxes are archived in Dryad: https://doi.org/10.5061/dryad.x69p8czt2.

Submitted 18 June 2024
Accepted 3 March 2025
Published 4 April 2025
10.1126/sciadv.adr1695